SATELLITE & MESOMETEOROLOGY RESEARCH PROJECT

Department of the Geophysical Sciences
The University of Chicago

UNPUBLISHED PRELIMINARY DATA

RESOLUTION OF THE NIMBUS HIGH RESOLUTION INFRARED RADIOMETER

by

Tetsuya Fujita
The University of Chicago

and

William Bandeen
Goddard Space Flight Center

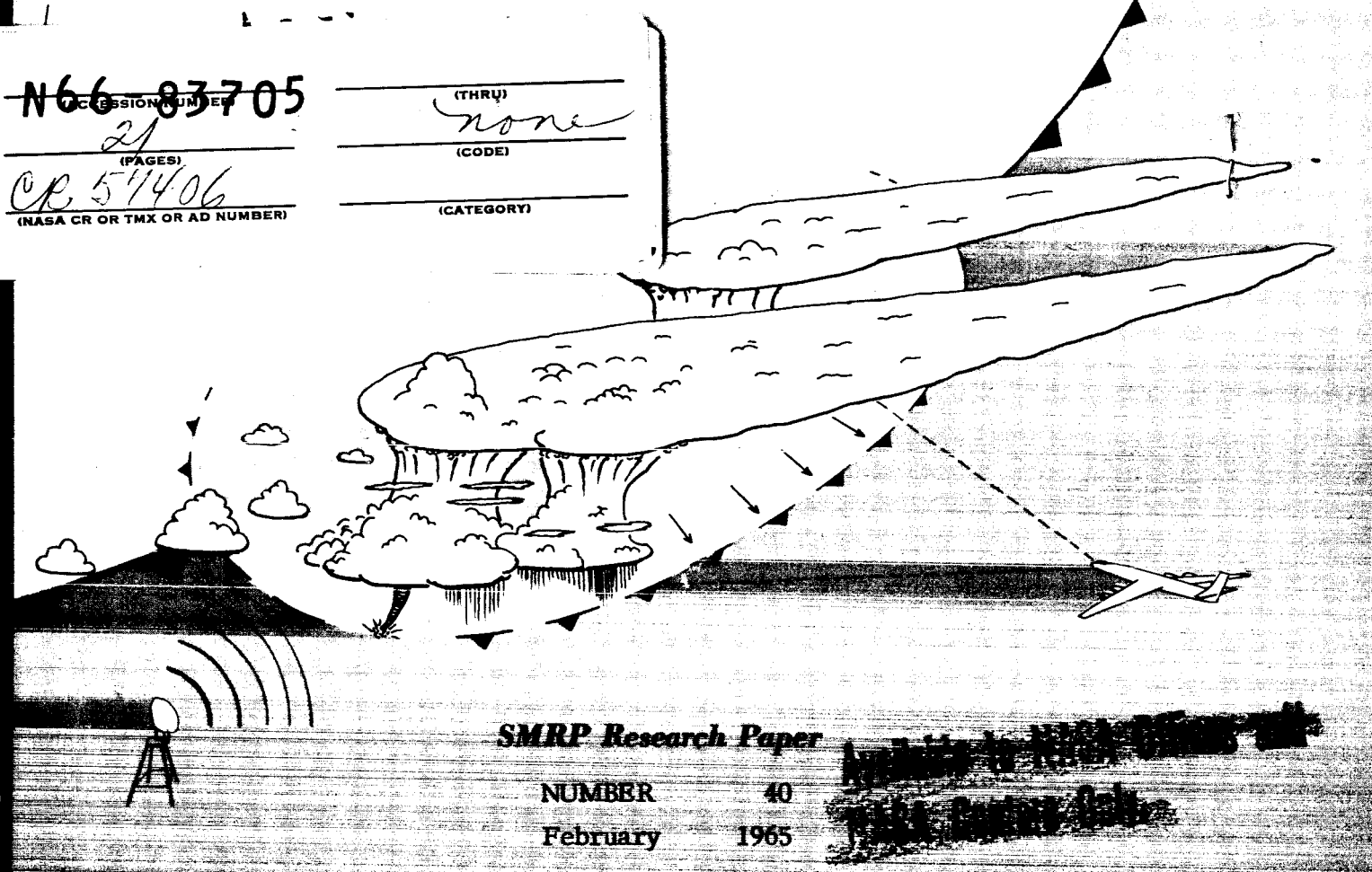

SMRP Research Paper
NUMBER 40
February 1965

MESOMETEOROLOGY PROJECT ---- RESEARCH PAPERS

1.* Report on the Chicago Tornado of March 4, 1961 - Rodger A. Brown and Tetsuya Fujita

2.* Index to the NSSP Surface Network - Tetsuya Fujita

3.* Outline of a Technique for Precise Rectification of Satellite Cloud Photographs - Tetsuya Fujita

4.* Horizontal Structure of Mountain Winds - Henry A. Brown

5.* An Investigation of Developmental Processes of the Wake Depression Through Excess Pressure Analysis of Nocturnal Showers - Joseph L. Goldman

6.* Precipitation in the 1960 Flagstaff Mesometeorological Network - Kenneth A. Styber

7.** On a Method of Single- and Dual-Image Photogrammetry of Panoramic Aerial Photographs - Tetsuya Fujita

8. A Review of Researches on Analytical Mesometeorology - Tetsuya Fujita

9. Meteorological Interpretations of Convective Nephsystems Appearing in TIROS Cloud Photographs - Tetsuya Fujita, Toshimitsu Ushijima, William A. Hass, and George T. Dellert, Jr.

10. Study of the Development of Prefrontal Squall-Systems Using NSSP Network Data - Joseph L. Goldman

11. Analysis of Selected Aircraft Data from NSSP Operation, 1962 - Tetsuya Fujita

12. Study of a Long Condensation Trail Photographed by TIROS I - Toshimitsu Ushijima

13. A Technique for Precise Analysis of Satellite Data; Volume I - Photogrammetry (Published as MSL Report No. 14) - Tetsuya Fujita

14. Investigation of a Summer Jet Stream Using TIROS and Aerological Data - Kozo Ninomiya

15. Outline of a Theory and Examples for Precise Analysis of Satellite Radiation Data - Tetsuya Fujita

* Out of print
** To be published

(Continued on back cover)

SATELLITE AND MESOMETEOROLOGY RESEARCH PROJECT
Department of the Geophysical Sciences
The University of Chicago

RESOLUTION OF THE NIMBUS HIGH RESOLUTION INFRARED RADIOMETER

by

Tetsuya Fujita
The University of Chicago

and

William Bandeen
Goddard Space Flight Center

SMRP Research Paper #40
February 1965

The research reported in this paper has been supported by the National Aeronautics and Space Administration under grant NASA NsG 333.

RESOLUTION OF THE NIMBUS HIGH RESOLUTION INFRARED RADIOMETER

Tetsuya Fujita
Department of the Geophysical Sciences
The University of Chicago
Chicago, Illinois
and
William Bandeen
Goddard Space Flight Center
National Aeronautics and Space Administration
Greenbelt, Maryland

35930

ABSTRACT

For the purpose of evaluating the resolution of the High Resolution Infrared Radiometer (HRIR) flown on board the Nimbus I meteorological satellite, three cloud-free regions in the western United States - the Grand Canyon, Death Valley, and Sierra Nevada - were selected. Enlarged HRIR pictures and the analog frequency traces of the scan lines in the pictures were examined in an attempt to investigate the types of noise superimposed on the signals. Two types of noise which appear in periodic and oscillatory fashions were found. The latter can be eliminated by taking running-mean values at one-degree scan angle intervals. The equivalent blackbody temperatures thus obtained were analyzed over these three regions, leading to the determination of the apparent temperature lapse rate inside the Grand Canyon atmosphere and of the temperature of Lake Tahoe and other lakes in Sierra Nevada. Death Valley was found to be about 10C warmer than the surrounding desert area 5000 ft high. An attempt was also made to produce an HRIR picture with isoneph contours similar to the iso-echo presentation of radar pictures.

Authors

1. Introduction

Beginning with the first medium-resolution five-channel scanning radiometer flown on the TIROS II meteorological satellite, it became possible to map terrestrial radiation patterns with varying degrees of resolution. The TIROS II (1961) and TIROS III (1962) Radiation Data Catalogs present a number of computer-produced maps which print out

grid point averages of a number of individual measurements sampled automatically in the data reduction. These individual values for TIROS II, III, and IV were sampled for every 72 satellite clock cycles, 550 cps, thus producing data points for every 0.1309 sec. During the reduction of the TIROS VII radiation data, the sampling rate was doubled, thus producing data points for every 0.0655 seconds (TIROS VII Radiation Data Catalog and Users' Manual, 1964).

One scan period of the TIROS radiometer is identical to the vehicle's spin period, which is about 6 sec. That is to say, the sampling was made approximately at intervals of 8-deg scan angles for TIROS II, III, and IV or 4-deg scan angles for TIROS VII. The term scan angle (σ) used herein is defined by Fujita (1964a). The sampled data available in the form of data listings taken directly from the Final Meteorological Radiation Tapes (FMRTs) give better resolution than the grid print maps. Nevertheless, the resolution is limited mainly by the sampling frequency.

The highest possible resolution can, therefore, be obtained by working directly from analog traces of output frequencies as discussed by Nordberg (1961). Even though the analog traces include inevitable noise coming from amplification, transmission, etc., they present true signals leading to the estimation of radiation values integrated over the radiometer's field of view, which is about 5 deg. Such a field of view projected to the earth's surface while looking straight down from a 700-km height is a circular spot of about 60 km in diameter.

In order to determine both cloud cover and height from radiation data, it is desirable to reduce the scan-spot size to the horizontal dimensions of the nephsystems to be detected. Otherwise, the clouds occupy only a part of the scan spot, and the radiometer measures only the mixed energy radiated from both clouds and their background.

2. High Resolution Infrared Radiometer

A High Resolution Infrared Radiometer (HRIR) was flown on the Nimbus meteorological satellite launched on August 28, 1964 in a quasi-polar orbit with an inclination of 98.663°. Due to its unexpectedly large eccentricity, 0.03610, the heights of the perigee and apogee were, respectively, 423.22 km and 932.70 km. The anomalistic period corresponding to these heights is 98.314 min, resulting in nearly 15 orbits of the earth a day.

This retrogade orbit produces a precession rate of $+1.0562^{\circ}$ per day, which is slightly larger than the angular velocity of the mean sun on the celestial sphere.

Nevertheless, the movement of the orbital plane permitted near midday photography by the Advanced Vidicon Camera System (AVCS) and near midnight HRIR measurements during the 26-day useful lifetime of the spacecraft.

The -6 db field of view of the Nimbus HRIR is designed to be 0.45 deg, about one-tenth of that of the TIROS five-channel radiometer, the half-power field of view of which is approximately 5 deg. The HRIR scan spots while looking straight down from perigee and apogee heights are 3.3 km (2.1 mi) and 7.3 km (4.5 mi), respectively. The period of the mirror rotation which provides the scanning within the plane perpendicular to the vehicle's instantaneous motion vector in space is 1.341818 sec. During this scanning period, the sub-satellite point advances an average of 9.1 km (5.7 mi), resulting in a shifting of the scan line on the earth. Because the Nimbus height at the perigee turned out to be lower than the planned height of 500 nautical miles (926 km), except near the apogee, there generally exists a narrow gap between consecutive scan lines at the nadir, which is not scanned by the radiometer. This gap disappears as the nadir angle of view increases.

The spectral response of the HRIR extends between the wave lengths 3.5 and 4.1 microns. The energy passing through the optical system is received by a photoconductive lead selenide detector which is actuated by a modulated signal through a mechanical chopper. The output signal and timing reference are recorded on a tape with a capacity of recording 57 minutes of HRIR data in the forward direction and the same in the reverse direction. These forward and reverse records can be played back simultaneously at eight times the recording speed, taking about seven and one-eighth minutes. Through this increased playback rate, the recorded frequencies from the voltage-controlled oscillator also increase by the factor of eight. That is to say, the output frequency range of 8.25 to 10.0 kcs controlled by the radiometer's output voltage, ranging from 0 to -6 volts, changes to a range of 66 to 80 kcs during the readout.

The calibration of the HRIR is carried out in the laboratory, using a blackbody target to simulate the long-wave radiation which the orbiting radiometer would receive from the earth and its atmosphere. With the blackbody target filling the sensor field of view, the radiometer output voltage is recorded as the target temperature is varied over the range of temperatures expected from the earth and its atmosphere. Several calibration runs are made at different detector-cell temperatures ranging from -76.5C to -69.8C. With these data and additional calibration data from the temperature-compensated voltage controlled oscillator, it is possible to relate the playback frequencies to the calibration target temperatures for given parametric values of the detector-cell temperature. Thus, in a manner similar to that pertaining to TIROS

infrared measurements, as discussed, for example, in the TIROS IV Radiation Data Catalog and Users' Manual (1963), the Nimbus I HRIR measurements are given in terms of an equivalent temperature, T_{BB}, of a blackbody filling the field of view, which would evoke the same response from the radiometer as does the generally non-blackbody radiation emerging from the top of the atmosphere. The history of the detector-cell temperature, a necessary parameter in the data reduction, is also recorded on magnetic tape in the spacecraft and telemetered to the ground during an interrogation. (For a more detailed discussion of the radiometer and its calibration, see the Nimbus I High Resolution Radiation Data Catalog and Users' Manual - Volume 1, 1965).

3. Photographic Display and Analog Traces

Photographic maps of HRIR data can be produced on a photofacsimile recorder by modulating a light beam with the analog radiometer signal while the light beam moves transversely across a film strip in synchronization with the rotation of the scanning mirror on the spacecraft. At the same time, the film strip is advanced at approximately the rate of the scaled distance between terrestrial scan lines per mirror rotation to simulate the forward motion of the spacecraft in orbit.

The film plane on which the modulated point light produces cloud patterns according to the radiative energy is expressed by the scan angle (σ) vs. time (t) coordinates. The coordinates are identical to those used by Fujita (1964b) in printing out the radiation data from the TIROS satellites by means of a scanning printer, and termed by him the scan angle - time (sigma-t) coordinates.

Because of the fact that the terrestrial distance scanned with a fixed range of the scan angle increases with the increasing nadir angle of view, a packing of terrestrial objects appears near the first and second horizons.

An example of such an HRIR photograph from Orbit 73 over the western United States around local midnight on September 2, 1964 is shown in Fig. 1. The photograph includes the superimposed latitudes and longitudes at 5-deg intervals, as well as the landmarks and state lines. Seen to the left are the scan numbers that are numbered arbitrarily for identification purposes. The time in Greenwich Mean Time appears to the right. The scan angle increasing toward the second horizon to the right is given at 10-deg intervals. The scan angle 0 deg starts at the local zenith point, and 180 deg denotes the nadir point. The perinadir represents the scan point closest to the subpoint; that is to say, the subpoint and the perinadir coincide when the attitude control of NIMBUS is perfect.

This HRIR photograph reveals various meteorological and ground features that can be used in evaluating the resolutions and capabilities of the radiometer. Even though the scope of this paper does not permit a discussion of the mathematical and technical procedures used in obtaining the superimposed geographic grids, it may be assumed that the grids are fairly accurate. At midnight under a clear sky, the land surfaces covered in part with grasses and trees seem to be much colder than the ocean. Of interest are the four lakes - Lake Tahoe, Pyramid Lake, Walker Lake, and Mono Lake - that appear as four black dots clearly seen in the picture. The Colorado River valley, especially the Grand Canyon, is warmer than the north and south limbs. The Salton Sea in lower California is definitely warm, and so is Death Valley. Conventional thinking might cause one to conclude that there is a cold-air-packed valley bottom; however, it appears as a warm area in the picture. The Rocky Mountains in Colorado are gray consequently distinguishable from scattered clouds which are white, leading to the inference that the clouds are higher and, hence, colder than the mountains.

In an attempt to analyze the equivalent blackbody temperatures over selected areas in the photograph quantitatively, an analog trace including the entire video signals used in producing the picture was made on Kodak Linagraph Direct Print paper. The Linagraph paper was not fixed, necessitating its photographic reproduction under very dim lights.

Two typical traces thus photographed and enlarged are shown in Fig. 2. They represent scans 275 and 276 passing over Death Valley and the Grand Canyon. A careful comparison of the traces and the photograph with the help of the scan angles indicated below would permit identification of the hot spots. Sierra Nevada, on approximately the 150-deg scan angle, is cold, indicating about -10C.

Rather important features of these analog frequency traces are the two types of noises superimposed on the traces. The first one indicated as black dots is the noise which appears as dips in periodic fashion. On a photographic display, the dips appear as diagonal white lines separated by constant scan angle intervals. The second one is oscillatory in nature, giving an impression that the short-lasting oscillations are superimposed. When examined on a photograph, they are characterized by an alternation of black and white dots in varying grayness. These two types of noises are called periodic noise and oscillatory noise. The oscillatory noise has been identified as a 200 cps, 500-millivolt peak-to-peak background level present on the HRIR power line in the spacecraft. The periodic noise consists of sharp spikes occurring at the rate of 16 per second. Although it has not been definitely established, the origin of the periodic spikes is also suspected to be on the spacecraft. Extensive tests are now under way attempting to find the source of the two types of noise and to eliminate or reduce

their effects on another HRIR experiment scheduled to be flown on the next Nimbus spacecraft.

4. Resolution of the HRIR Data

The periodic noise superimposed on the HRIR analog signal does not interfere with the accuracy and resolution of the HRIR photograph. The oscillatory noise is, however, very difficult to detect unless either a photograph or an analog trace is enlarged and examined. One might still assume, however, that such an oscillatory trace could represent a true signal rather than noise.

For the purpose of clearing up the noise versus signal debate, enlarged traces from scans 275 and 276 were placed over the topographic profile following the scan lines along which the actual scanning took place (Fig. 3). As shown in Fig. 2, scan 275 is rather free from oscillatory noise but scan 276 is extremely noisy over the Death Valley region. The scan lines are separated by only about 10 km yet the nature of the two traces is quite different. The black spots placed on a scan line denote the scan spots in Fig. 3.

An enlarged photograph in Fig. 4. covers the area of the two scan lines under discussion. The numbers 1 through 23 entered at the white or gray spots in the picture correspond exactly to the minimum temperatures on the analog traces in Fig. 3, in which temperatures increase downward.

An attempt has been made to apply a running mean method to suppress the oscillatory noise while preserving the signals. Starting from a noisy trace from scan 276, a series of running means of the equivalent blackbody temperature was computed by

$$\overline{T}_{BB}(\sigma, \Delta\sigma) = \frac{1}{\Delta\sigma} \int_{\sigma - \frac{1}{2}\Delta\sigma}^{\sigma + \frac{1}{2}\Delta\sigma} T_{BB}\, d\sigma \qquad (1)$$

where σ denotes the scan angle and $\Delta\sigma$, the interval of the running means. Figure 5 represents the results obtained by setting $\Delta\sigma$ to $1/2^{\circ}$, 1°, 2°, and 4°. By increasing $\Delta\sigma$, it is seen that the oscillatory noise is first suppressed, then eliminated after $\Delta\sigma = 2^{\circ}$. At the same time the running-mean curve tends to lose its gradient if $\Delta\sigma$ is increased over 1 deg. Careful comparison of the running-mean curves and the ground profile leads to the conclusion that a 1-deg running mean would be the best, since it would eliminate most of the oscillatory noise while preserving the temperature gradient expected from the ground profile.

5. Mapping with One-Degree Running-Mean Temperatures

For the purpose of testing the results of the mapping of the equivalent blackbody temperatures after the one-deg running mean has been applied, an area surrounding Lake Tahoe in Sierra Nevada was selected. An enlarged picture in Fig. 6, rather like the Ranger 7 moon picture in appearance, shows Lake Tahoe and Walker and Mono Lakes as dark areas. The largest one, Lake Tahoe, covers no more than a 15 x 20 mi area.

By using a calibrated analog trace, one-deg running-mean temperatures were obtained from the scans 245 through 261. The equivalent blackbody temperatures were then plotted on a local map to detect variations associated with the lakes (dark stippled areas) and with dry salt-lake beds (light stippled areas). Figure 7 reveals that Lake Tahoe with +8C near the center is surrounded by a -2C to -10C cold region representing mountains around the lake. Walker Lake is also warm, showing +11C at the lake center. Mono Lake, the smallest yet detected, was scanned by only one scan line, No. 260, showing a +6C temperature. It will be found that only one scan line on the HRIR picture produced a small dark area representing this lake.

These equivalent blackbody temperatures are analyzed in Fig. 8. The 2C-interval isotherms clearly represent lakes in Sierra Nevada if their diameters are ten miles or larger. The dry lake beds near the northeast corner of the chart are a few degrees warmer than their surroundings. It is rather difficult, however, to conclude whether the beds are warmer than the ordinary ground. The fact that they exist in low land, which would provide higher equivalent blackbody temperatures, might give a few degrees warmer temperature.

The scatter diagram presented in Fig. 9 includes all the temperature values in Fig. 7 plotted against the ground height. Small black dots, open circles, and large painted circles, respectively, denote the regular ground, dry salt-lake beds, and water-filled lakes. The ground temperature can be approximated by a straight line. The lapse rate given by this straight line is about $6^{o}km^{-1}$. A line parallel to this straight line can be drawn through the highest lake temperatures. This line would represent the lake temperature, less atmospheric absorption, since the number of painted circles with lower temperatures represent mixtures of the land and lake temperatures. It is seen that Lake Tahoe and Mono Lake are colder than Pyramid and Walker Lakes, as the ground-temperature lapse rate indicates.

6. Temperature of the Grand Canyon

The HRIR picture of Fig. 1 shows a meandering dark line along the Colorado River superimposed on the picture. Since the Colorado River, dammed up in several locations, runs through deep gorges and canyons, we might suspect that the dark line represents the warm canyon bottom which is large enough to include most of the radiometer's scan spot when the radiometer axis is oriented toward the center of the canyon.

The deepest canyon, the Grand Canyon in Arizona, was selected for detailed investigation of equivalent blackbody temperatures. An enlarged view of the canyon, including about 10 scan lines, appears in Fig. 10. Both the Grand Canyon and Lake Mead as well as the periodic noise are identified in the picture. It should be noted that the oscillatory noise along several scan lines is appreciable and that the noise may be present on one scan line but not on the adjacent one.

One-deg running means were applied to obtain the equivalent blackbody temperatures which are plotted and analyzed in Fig. 11. The plotted temperature values appear only along the canyon floor, thus describing the plateau temperature by the isotherms contoured for every two deg Centigrade.

The mean temperatures are also plotted on an aerial picture of the Grand Canyon taken by one of the authors from a Continental Airlines jet on November 30, 1964 (Fig. 12). The equivalent blackbody temperatures in deg Centigrade along four scan lines 264 through 267 clearly indicate the variations as the sensor axis moves over the deep canyon from left (West) to right. The Nimbus moved from the top to the bottom of the picture while scanning the canyon area at about 1.34-sec intervals.

The temperature of the Grand Canyon floor was about 14C, while the Canyon rim about 5000 ft above the floor showed 0C to 3C temperature. This would result in a lapse rate of about 10C km^{-1}, the dry adiabatic lapse rate. We are, of course, not measuring the air temperatures on the rim and the floor. The equivalent blackbody temperatures obtained are rather a measure of the radiative temperatures at the surface, modified slightly by the atmospheric absorption and emission between the source and the satellite. The surface radiative temperatures, in turn, are a function of both the kinetic temperatures and emissivities of the surface materials, within the effective spectral response interval of the radiometer ($\sim 3.5\mu - 4.1\mu$). If we assume, however, that the difference between the air near the surface and the underlying ground temperatures is the same at the rim and the floor and that the emissivities of the surface materials are the same and approach unity (i. e., the radiating properties of the materials approach those of a blackbody), we may assume that the lapse rate of the equivalent blackbody temperatures represents that of the air temperature. If the differential absorption by the

moisture between the floor and the rim were considered, it would tend to make this inferred lapse rate even larger.

What is the reason for the dry- or super-adiabatic lapse rate inside the Grand Canyon atmosphere? We may first suspect that the water in the Colorado River is warmer at midnight than the rocks on the canyon floor. The fact that Lake Mead temperature is slightly colder than the canyon floor temperature rules out this suspicion. Besides the width of the Colorado River in the Grand Canyon is normally so narrow that it would not contribute appreciably to the integrated radiance viewed by the satellite.

Protective effects of the mile-high walls of the canyon for outgoing radiation might have something to do with the prevention of nocturnal radiation loss. In order to prove such an effect, it is necessary to make profiles of the canyon in an attempt to compute the radiation loss as a function of the locations along the Colorado River.

Another way of interpreting such a large lapse rate is the dry-adiabatic warming of the cold air from the rim as it descends along the wall to the canyon floor. Pictures of descending fog or stratus from the Grand Canyon rim are seen in various magazines; however, the ones photographed by Tallon (1964) show spectacular views of the ground fog falling from the rim into the canyon. The descending air reaching almost to the canyon bottom will be continuously drained toward Lake Mead. In fact, the relatively low temperature of this lake surface might be explained by the cold drainage wind sweeping over the lake surface at night. Such a circulation, involving dry-adiabatic descent and drainage, seems entirely possible in the Grand Canyon atmosphere.

Of course we must not reject the possibility that our basic assumptions are in error. First, a strong nocturnal surface inversion at the rim without a comparable inversion at the canyon floor would lead to an erroneously large free-air lapse rate inferred from the HRIR data. Second, a lower surface emissivity at the rim than at the canyon floor would also lead to an erroneously large free-air lapse rate inferred from the HRIR data. It appears that it would be most useful to investigate all of the possibilities discussed above by establishing a mesometeorological network in the Grand Canyon area.

7. Iso-neph Presentation of HRIR Data

Techniques for automatic depiction of two or more contours of radar echoes developed by Atlas (1947) permit radar observers to identify the areas of intense return from a cluster of saturated echoes. Since then the iso-echo presentation of thunderstorms has been utilized by various operational and research groups. Atlas

technique gives additional gray scales in photographic presentations if the levels of the iso-echo are properly selected.

In the photographic presentation of the HRIR neph patterns, a similar principle can be applied. The colder clouds within certain temperature ranges appear whiter on the photograph; however, a reverse radiance level can be set to that of very cold clouds in such a manner that the areas of very cold cloud are reproduced in almost saturated black. Unlike the case of radar echoes, the gradient of the equivalent blackbody temperature near the high cloud edge is, in many cases, so great that it may not be practicable to modulate lights within the area of these cold clouds. Figure 13 was produced by superimposing an overdeveloped high-contrast negative on the underdeveloped low-contrast positive film. Because the high-contrast negative was not able to cut off the light sharply along the cloud edge, the coldest clouds are not well-defined. Nevertheless, the picture represents a simulated picture of future HRIR data with an iso-neph contour presentation.

8. Conclusions

The Nimbus-borne HRIR data have shown a great improvement over TIROS medium-resolution data in terms of their resolution and the number of the scan spots per unit area on the earth. The analog records of play-back frequencies include some noise, but most of it can be eliminated by taking running means at one-degree scan angle intervals.

Analysis of the mean equivalent blackbody temperatures thus obtained revealed various radiative features of the cloud-free terrain near midnight. Such a detailed analysis should be performed over the area of nephsystems associated with various meteorological disturbances such as thunderstorms, squall-lines, hurricanes, etc. It has been found that combined analyses of HRIR pictures and analog traces can be made for research purposes if the local areas for study are carefully selected.

Acknowledgements: We should like to acknowledge the assistance of Mr. Lonnie Foshee, the Goddard Space Flight Center Experimenter, for kindly making the data discussed in this paper available to us. We are also grateful to the staff members of the Satellite and Mesometeorology Research Project of the University of Chicago for various assistance toward the completion of this paper.

REFERENCES

Atlas, D., 1947: Preliminary report on new techniques in quantitative radar analysis of rainstorms. Rep. AWNW 7-4, Part I (Dayton, Ohio: A.M.C., Wright-Patterson A.F.B.)

Fujita, T., 1964a: A technique for precise analysis of satellite data. Vol. II - radiation analysis. SMRP Res. Paper 29, 107-126.

_____, 1964b: The scanning printer and its application to detailed analysis of satellite radiation data. SMRP Res. Paper 34, 29 pp.

Nimbus I High Resolution Radiation Data Catalog and Users' Manual - Volume 1. Photo-fascimile Film Strips, 1965 NASA: Goddard Space Flight Center, Greenbelt, Maryland. (To be published).

Nordberg, W., 1961: Physical measurements and data processing. Abstracts and figures of lectures, The International Meteorological Satellite Workshop, Washington, D. C., 107-120.

Tallon, J., 1964: Ground fog in Grand Canyon. Arizona Highways. Vol. XL-12, Phoenix, Arizona.

TIROS II Radiation Data Catalog, 1961: NASA, Goddard Space Flight Center, Greenbelt, Maryland, 356 pp.

TIROS III Radiation Data Catalog, 1962: NASA, Goddard Space Flight Center, Greenbelt, Maryland, 388 pp.

TIROS IV Radiation Data Catalog and Users' Manual, 1963: NASA, Goddard Space Flight Center, Greenbelt, Maryland, 250 pp.

TIROS VII Radiation Data Catalog and Users' Manual - Volume 1, 1964: NASA, Goddard Space Flight Center, Greenbelt, Maryland, 255 pp.

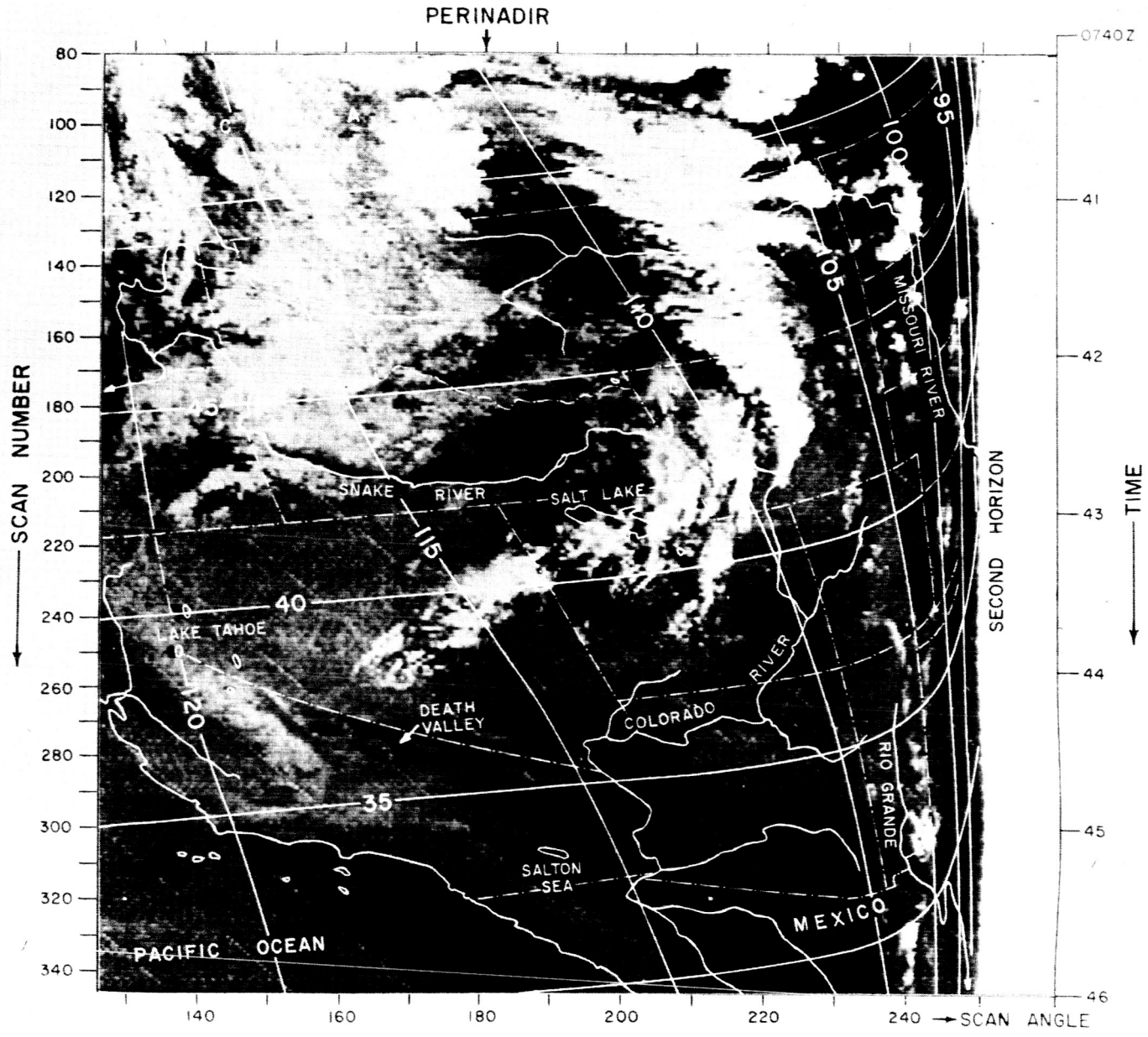

Fig. 1. HRIR picture of the Western United States obtained by Nimbus I during Orbit 73, September 2, 1964. The satellite moved from Montana to California at the heights 0740Z (448 km), 0742Z (438 km), 0744Z (432 km), and 0746Z (431 km). The radiometer's scanning direction is clockwise when seen from the rear of the satellite.

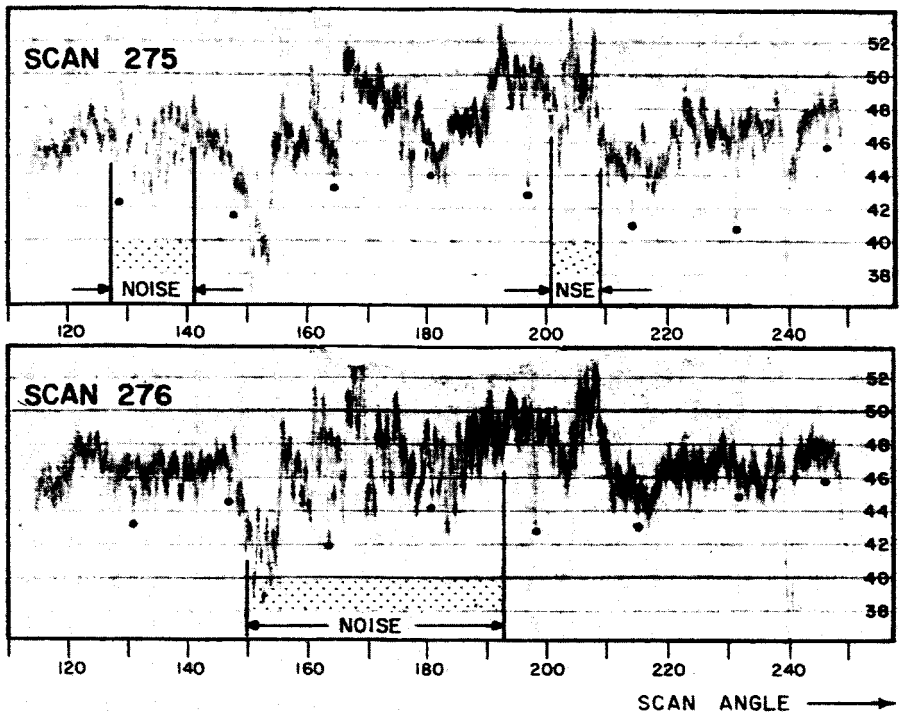

Fig. 2. Enlarged analog traces from scans 275 and 276. The chart includes the numbered lines which correspond to various equivalent blackbody temperatures as follows: Line number 38 (temperature -10.0C), 40 (-7.0C), 42 (-3.5C), 44 (0.0C), 46 (3.8C), 48 (8.0C), 50 (12.5C), and 52 (17.0C). Black dots are periodic noise and the intervals of the oscillatory noise are indicated by stipplings.

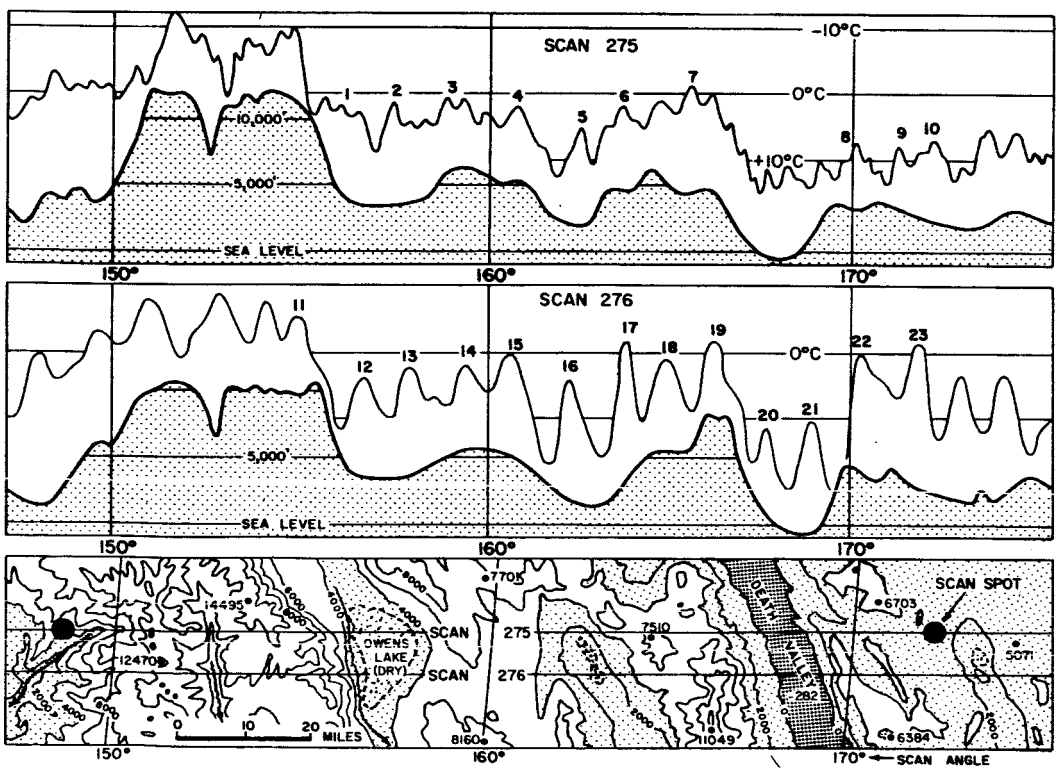

Fig. 3. Two analog traces placed over the topography profiles along the scan lines corresponding to these traces. The upper trace from scan 275 is relatively free from noise, but the lower one is characterized by a significant oscillatory noise superimposed on the signal. The wave length of the oscillatory noise is equivalent to about 1.3 deg of the scan angle.

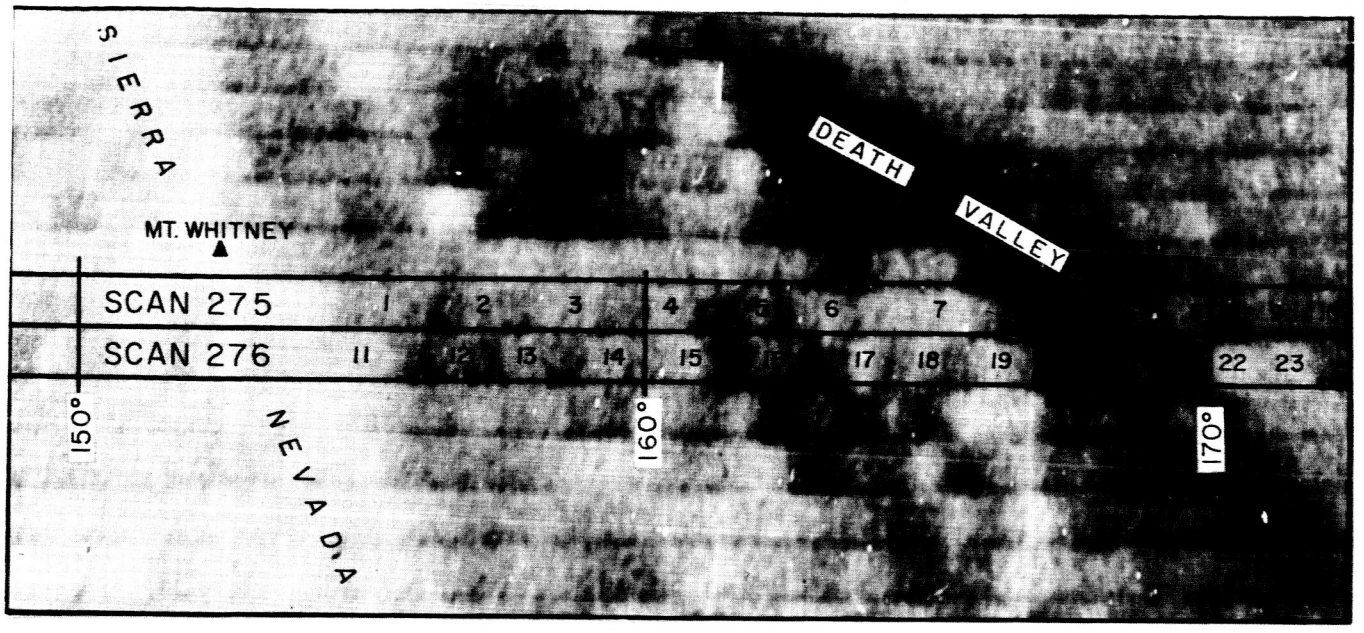

Fig. 4. Enlarged HRIR picture showing Sierra Nevada and Death Valley. The equivalent blackbody temperatures of Mt. Whitney, 14,495 ft, and Death Valley, -282 ft, the highest and the lowest points in the U.S., were -12C and +15C, respectively. Numbers 1 through 23, identifying gray spots on the scan lines, correspond to those of the minimum temperatures along the analog traces in Fig. 3.

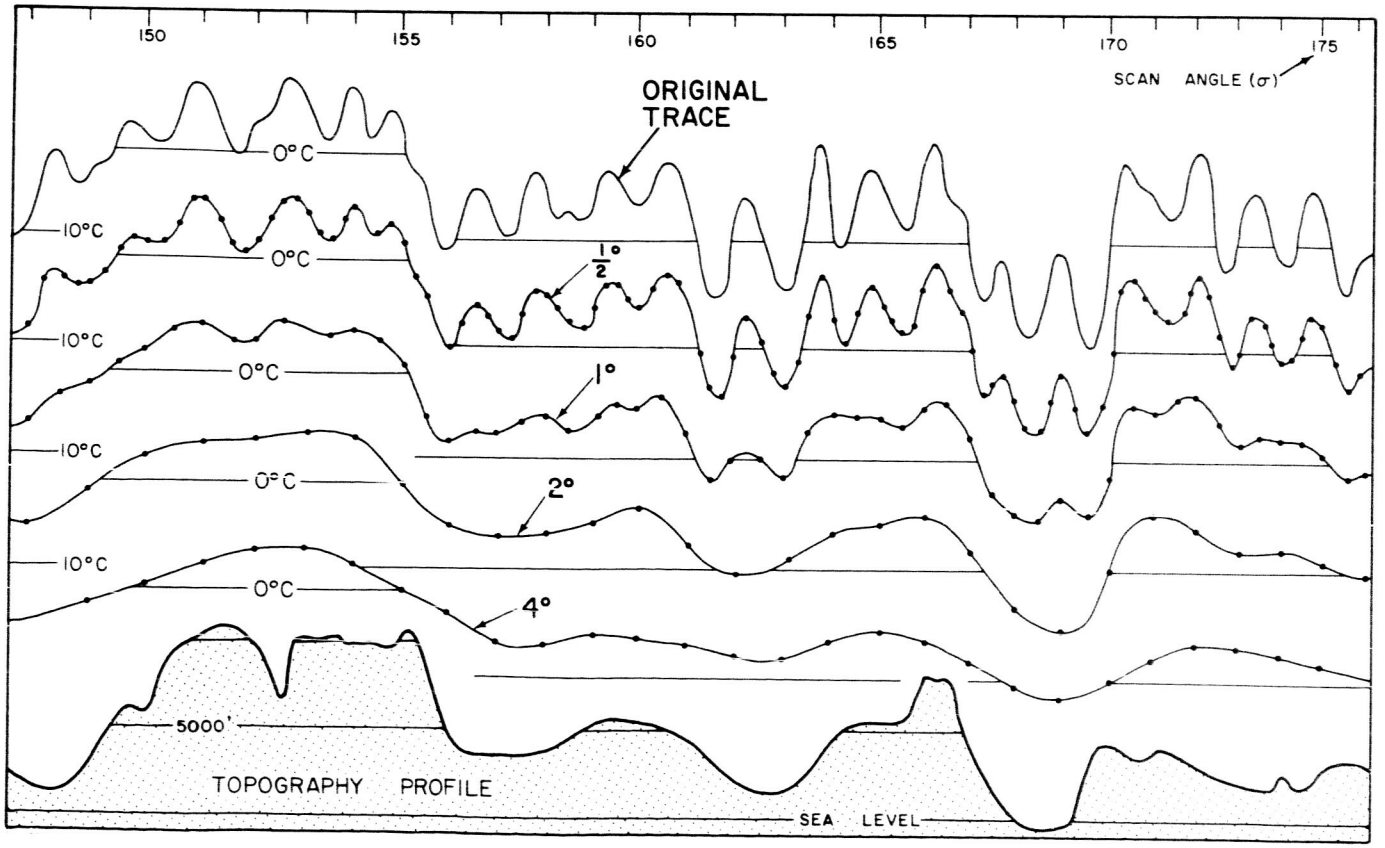

Fig. 5. Suppression of oscillatory noise by computing running-mean temperatures for various scan-angle intervals. These curves imply that the one-deg mean is the best for noise suppression while keeping the signals unsmoothed.

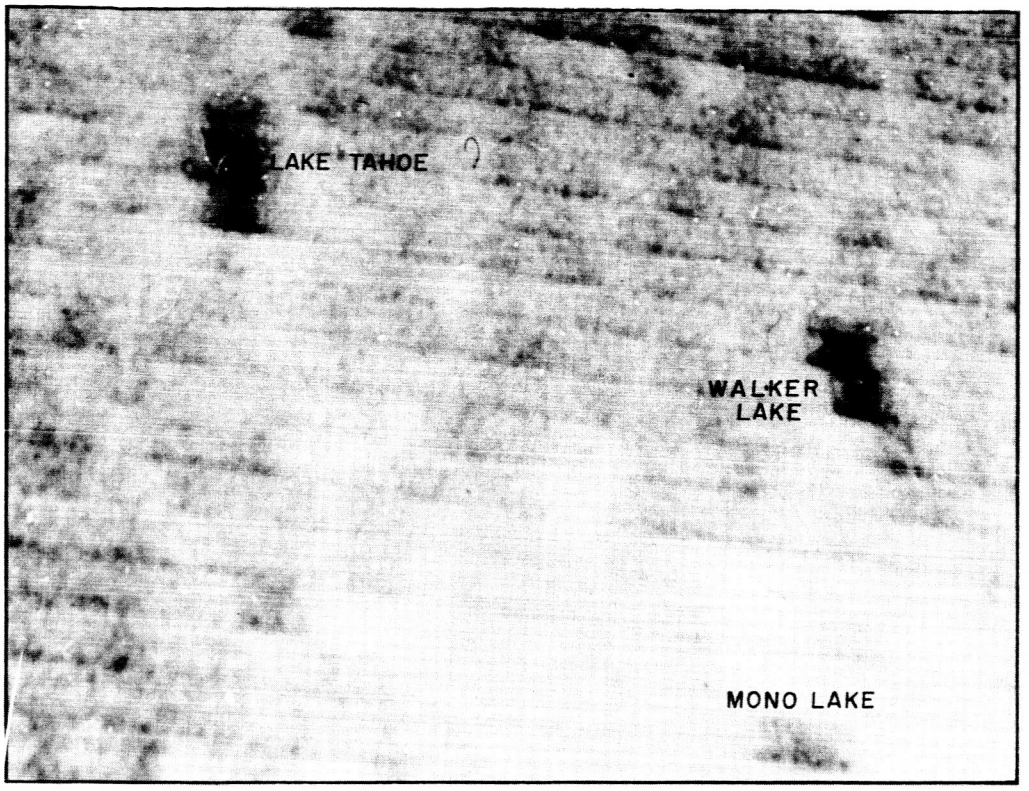

Fig. 6. HRIR picture showing the three lake regions in Sierra Nevada. Three dark spots looking somewhat like small craters in Ranger 7 pictures are Lake Tahoe, Walker Lake, and Mono Lake. These lakes are found to be about 11C warmer than the surrounding mountains.

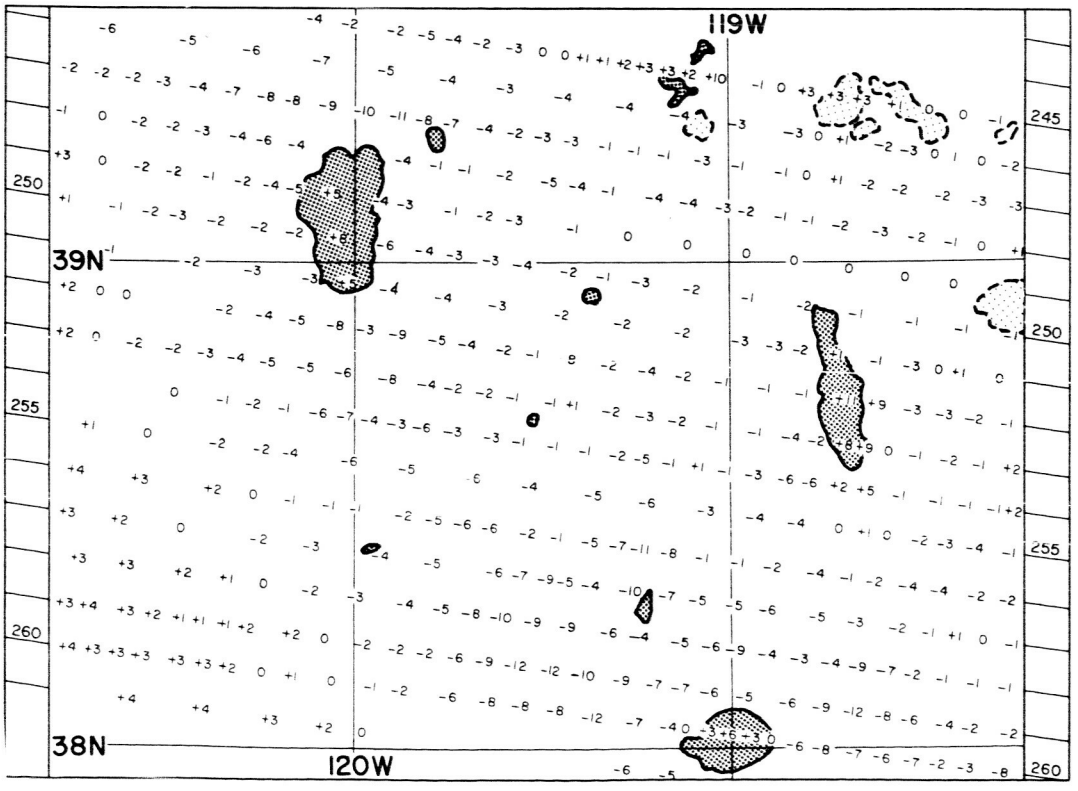

Fig. 7. Mean equivalent blackbody temperatures computed by taking running means of the analog traces at one-deg scan angle intervals.

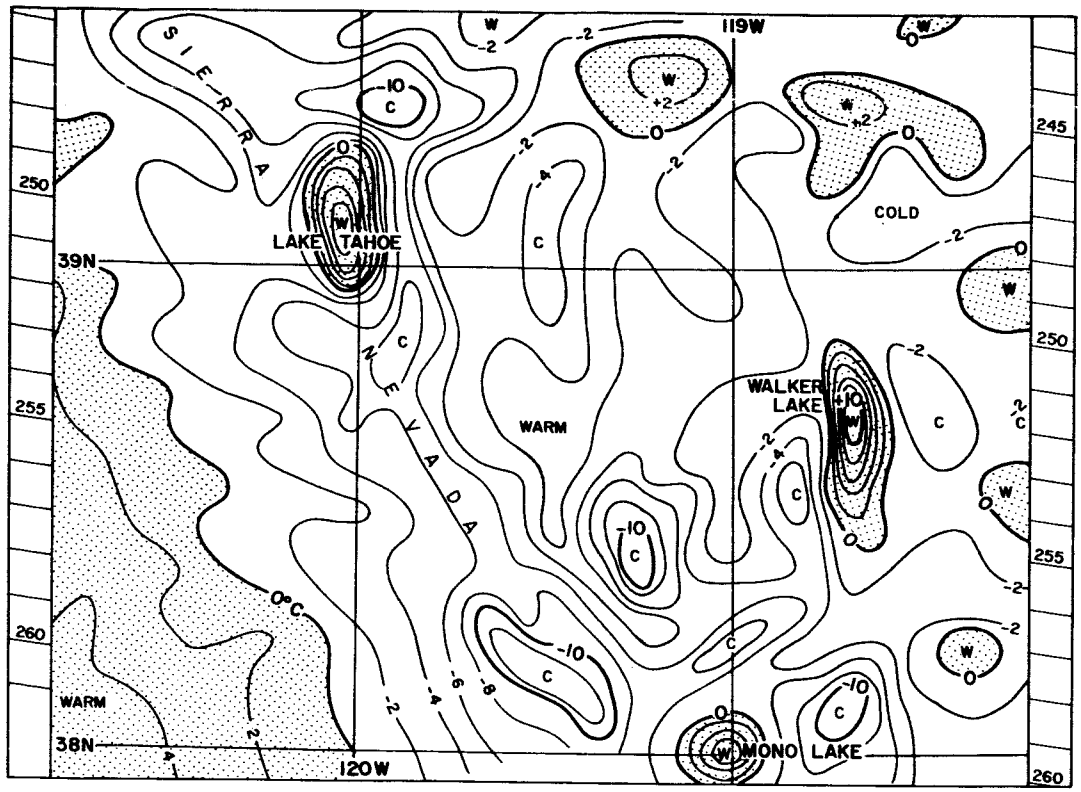

Fig. 8. Isotherms of the mean equivalent blackbody temperatures. Note Lake Tahoe is a few degrees warmer than the ground in the San Joaquin Valley, California.

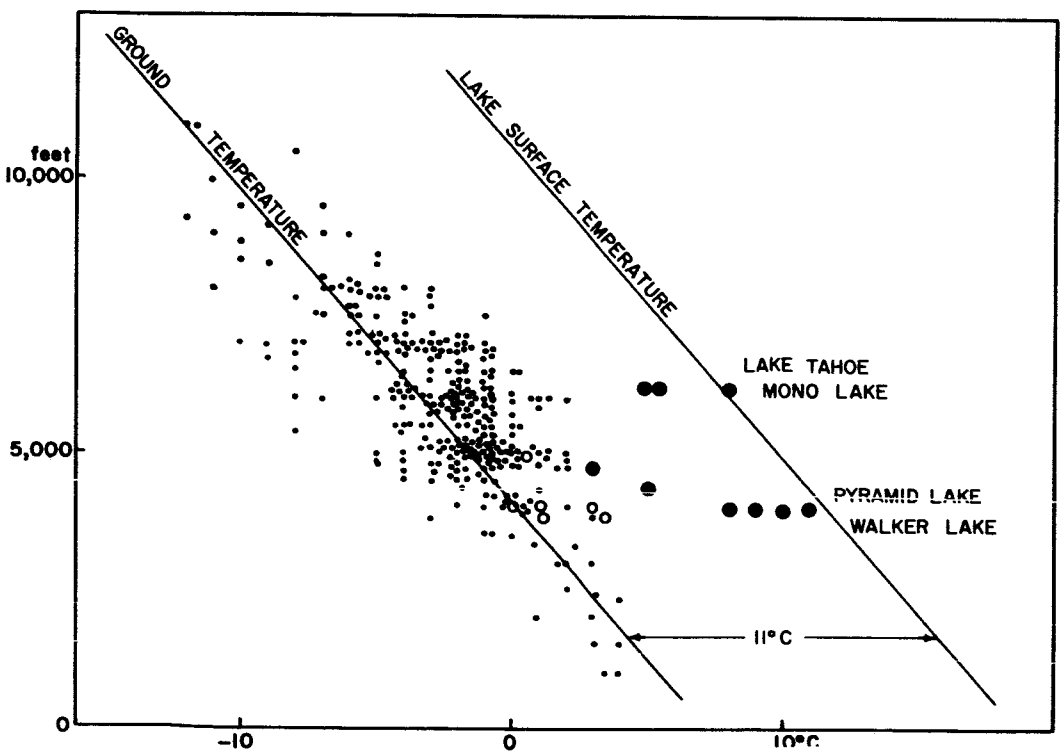

Fig. 9. Scatter diagram showing the equivalent blackbody temperatures plotted against the elevation of each scan spot. Small dots represent ground surface; open circles, dry lake beds; and painted circles, the mixture of lake and ground surfaces. Data from Sierra Nevada were taken near Lake Tahoe.

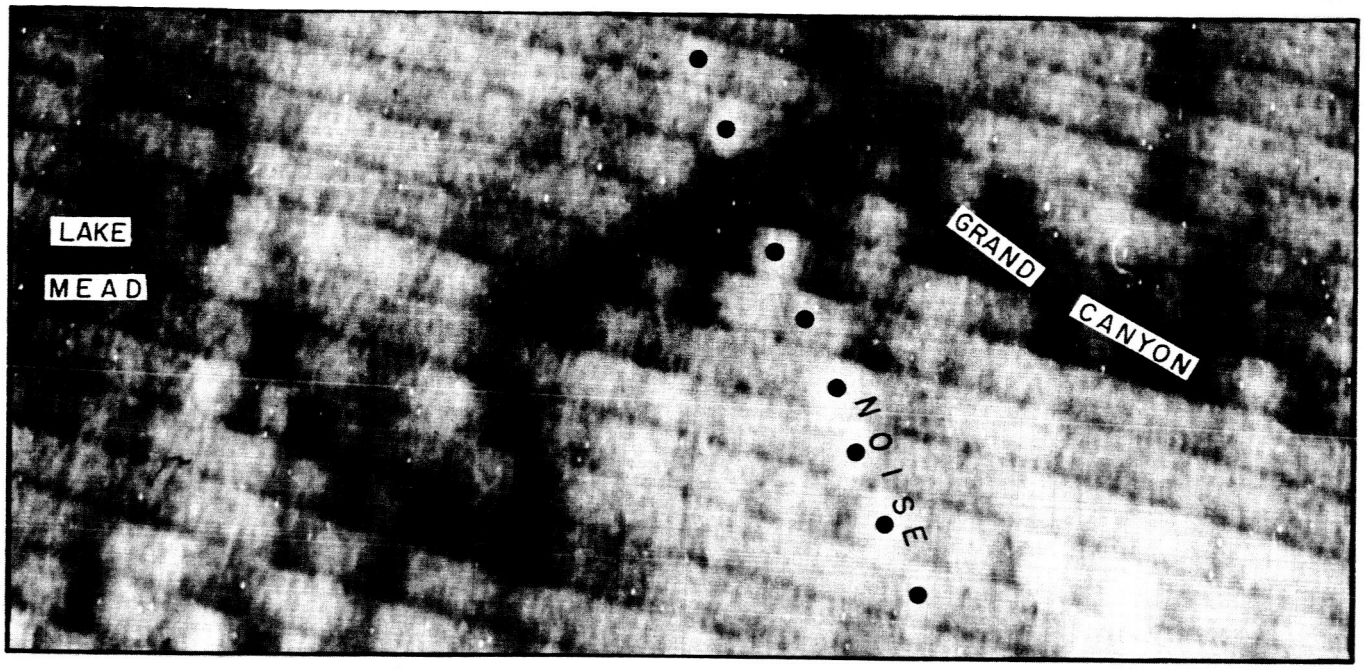

Fig. 10. Enlarged view of Grand Canyon and Lake Mead area portrayed by the HRIR picture. Black dots represent periodic noise which should be disregarded.

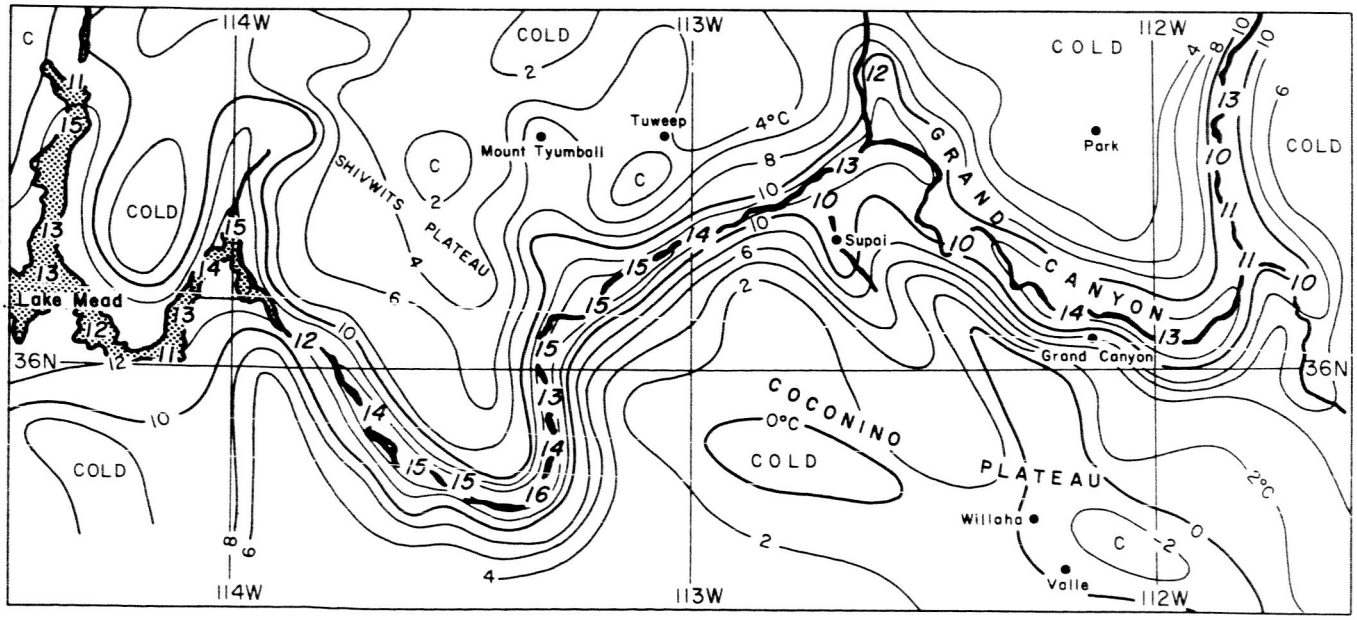

Fig. 11. Canyon floor and Lake Mead temperatures indicated by slant letters. Equivalent blackbody temperature of the canyon rim and plateau is shown by the isotherms contoured for every 2C.

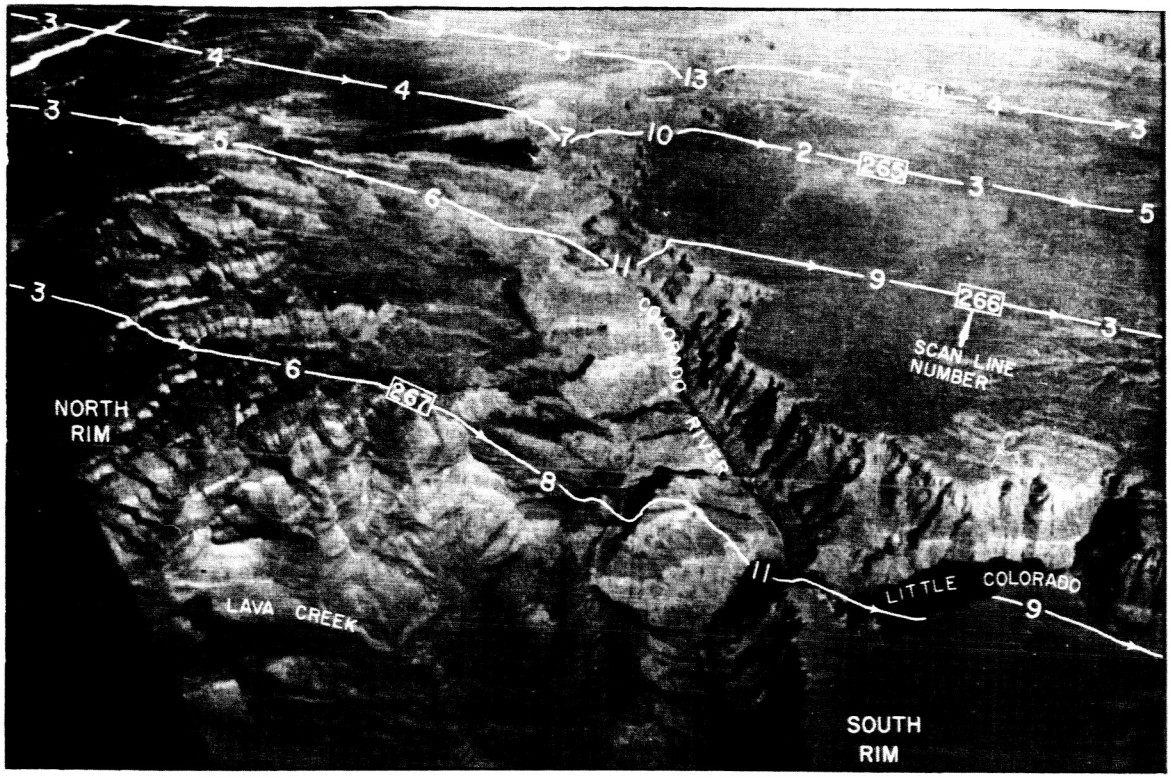

Fig. 12. Scan lines and equivalent blackbody temperatures superimposed on an aerial picture of the Grand Canyon. Aerial picture: from Continental Airlines Jet from Chicago to Los Angeles at 11 AM, MST, November 30, 1964, altitude 33,000 ft. Nimbus data: 0044 MST, September 2, 1964 from 432-km altitude.

Fig. 13. Iso-neph presentation of HRIR picture from Nimbus Orbit 73, September 2, 1964, showing a small tropical disturbance in the Pacific Ocean off the Mexican coast. In this presentation, extremely cold clouds inside the saturated white areas are shown as black areas. This picture was made by superimposing both positive and negative films on a photographic paper while making a contact print.

MESOMETEOROLOGY PROJECT - - - - - RESEARCH PAPERS

(Continued from front cover)

16. Preliminary Result of Analysis of the Cumulonimbus Cloud of April 21, 1961 -Tetsuya Fujita and James Arnold

17. A Technique for Precise Analysis of Satellite Photographs - Tetsuya Fujita

18. Evaluation of Limb Darkening from TIROS III Radiation Data - S.H.H. Larsen, Tetsuya Fujita, and W. L. Fletcher

19. Synoptic Interpretation of TIROS III Measurements of Infrared Radiation -Finn Pedersen and Tetsuya Fujita

20. TIROS III Measurements of Terrestrial Radiation and Reflected and Scattered Solar Radiation - S.H.H. Larsen, Tetsuya Fujita, and W.L. Fletcher

21. On the Low-level Structure of a Squall Line - Henry A. Brown

22. Thunderstorms and the Low-level Jet - William D. Bonner

23. The Mesoanalysis of an Organized Convective System - Henry A. Brown

24. Preliminary Radar and Photogrammetric Study of the Illinois Tornadoes of April 17 and 22, 1963 - Joseph L. Goldman and Tetsuya Fujita

25. Use of TIROS Pictures for Studies of the Internal Structure of Tropical Storms -Tetsuya Fujita with Rectified Pictures from TIROS I Orbit 125, R/O 128 -Toshimitsu Ushijima

26. An Experiment in the Determination of Geostrophic and Isallobaric Winds from NSSP Pressure Data - William Bonner

27. Proposed Mechanism of Hook Echo Formation - Tetsuya Fujita with a Preliminary Mesosynoptic Analysis of Tornado Cyclone Case of May 26, 1963 -Tetsuya Fujita and Robbi Stuhmer

28. The Decaying Stage of Hurricane Anna of July 1961 as Portrayed by TIROS Cloud Photographs and Infrared Radiation from the Top of the Storm -Tetsuya Fujita and James Arnold

29. A Technique for Precise Analysis of Satellite Data, Volume II - Radiation Analysis, Section 6. Fixed-Position Scanning - Tetsuya Fujita

30. Evaluation of Errors in the Graphical Rectification of Satellite Photographs -Tetsuya Fujita

(Continued on outside)

MESOMETEOROLOGY PROJECT - - - - - RESEARCH PAPERS
(Continued from inside)

31. Tables of Scan Nadir and Horizontal Angles - William Bonner

32. A Simplified Grid Technique for Determining Scan Lines Generated by the TIROS Scanning Radiometer - James Arnold

33. A Study of Cumulus Clouds over the Flagstaff Research Network with the Use of U-2 Photographs - Dorothy L. Bradbury and Tetsuya Fujita

34. The Scanning Printer and Its Application to Detailed Analysis of Satellite Radiation Data - Tetsuya Fujita

35. Synoptic Study of Cold Air Outbreak over the Mediterranean Using Satellite Photographs and Radiation Data - Aasmund Rabbe and Tetsuya Fujita

36. Evaluation of Doppler Navigation Using Photogrammetric Methods of Position Fixes - Tetsuya Fujita with Robbi Stuhmer

37. Proposed Operation of Instrumented Aircraft for Research on Moisture Fronts and Wake Depressions - Tetsuya Fujita and Dorothy L. Bradbury

38. Statistical and Kinematical Properties of the Low-Level Jet Stream - William D. Bonner

39. The Illinois Tornadoes of 17 and 22 April 1963 - Joseph L. Goldman